Interpretation of the Cross Correlation Function of STEREO Solar Wind Velocities using a Global MHD Model

Pete Riley[1], J. A. Linker[1], Z. Mikic[1], J. Luhmann[2], and A. Opitz[3]

————

[1]Predictive Science, San Diego, California,

USA.

[2]SSL, University of California Berkeley,

California, USA.

[3]Centre dEtude Spatiale des

Rayonnements (CNRS-UPS), University of

Toulouse, Toulouse, France.

Abstract.   The unique trajectories of the STEREO A and B spacecraft

are allowing an unprecedented view of the structure of the three-dimensional

heliosphere. One aspect of this is the degree to which the measurements at

one spacecraft correlate with those at the other. We have computed the cross

correlation function (CCF) for STEREO *in situ* observations of the bulk so-

lar wind velocity as the spacecraft moved progressively farther away from

one another. Our results confirm previous studies that the phase lag between

the signals becomes linearly larger with time. However, we have identified

two intervals where this appears to break down. During these "lulls," the CCF

reveals a phase lag considerably less than that which would be predicted based

only on the angular separation of the spacecraft. We modeled the entire STEREO

time period using a global MHD model to investigate the cause for these "lulls."

We find that a combination of time-dependent evolution of the streams as

well as spatial inhomogeneities, due to the latitudinal separation of the space-

craft, are sufficient to explain them.

1. Introduction

The STEREO (Solar Terrestrial RElations Observatory) mission launched on October 25th, 2006 on a Delta II rocket. Since early 2007, it has been continuously returning a wide range of remote solar and *in situ* measurements of the Sun's corona and the inner heliosphere. Charged with a number of fundamental scientific objectives, one of particular relevance to this study is to improve our understanding of the structure of the ambient solar wind. With nearly identical instrumentation, the STEREO ahead (A) and behind (B) spacecraft are separating by $\sim 45°$ per year. Restricted to the ecliptic plane, in addition to the monotonically-increasing longitudinal separation, the spacecraft also separate from one another in heliographic latitude, up to a maximum separation of $\sim 14.4°$. The measurements from STEREO A and B thus represent a unique dataset from which to study the effects of spatial and temporal evolution of solar wind streams, and, in particular, to assess the degree of correlation between them.

Previous studies have investigated the correlation of solar wind stream structure from one and multiple spacecraft. The first comprehensive auto-correlation analysis of *in situ* solar wind data was performed by *Gosling and Bame* [1972]. Using solar-wind speed data from the Vela 2 and 3 missions, they assessed to what extent solar wind structure persisted from one rotation to the next. They found that the average correlation was only 0.3, suggesting that most structure did not persist from one rotation to the next; However, this coefficient varied from 0.1 to 0.7 at different times. They also noted that differential rotation affected the results, the implication being that a wide range of helio-latitudes contributed to the solar wind measured at Earth. In a more comprehensive

analysis, *Gosling et al.* [1976] found that the most stable stream structure occurred during the declining phase of the solar cycle. *Richardson et al.* [1998] cross-correlated data from ISEE 3 at L1 and IMP 8 at Earth for times corresponding to near-solar maximum conditions. They found that the temporal lag between the structures observed at the two spacecraft depended on both the radial and azimuthal separation. Additionally, they found that the lag required a correction due to corotation, that is, that the stream normals are tilted away from the radial direction and toward the direction of planetary motion. In contrast, *Paularena et al.* [1998], investigating the correlation between data observed by IMP 8, Interball-1, and Wind during near-solar minimum conditions, found that the correlation depended only on the radial separation of the spacecraft and not on the azimuthal separation. Moreover, they did not find any need to correct for corotation. *Richardson et al.* [1998] suggested that the smaller angular separation of the spacecraft in the *Paularena et al.* [1998] study, together with the fact that the two investigations used data from different extremes of the solar cycle could account for these apparent contradictions.

Podesta et al. [2008] first reported on the correlation length of large-scale solar wind velocity fluctuations measured at STEREO A and B. They focused on the interval between February 2007 and August 2007, corresponding to near-solar minimum conditions. They found that the transverse correlation length was 0.25±0.02 AU. *Opitz et al.* [2009] analyzed the solar wind velocity from STEREO A and B from March to August of 2007. Their study focused on the temporal evolution of the solar wind at the two spacecraft by removing spatial effects caused by the radial and angular separation of the two spacecraft. In particular, they time-shifted STEREO B, accounting for both longitudinal and radial

63 separation and computed the correlation coefficient between it and STEREO A data.

64 They found that the correlation decreased with increasing separation (and time). However,

65 they noted some exceptions to the otherwise good correlations found: (1) Day 142, 2007,

66 which coincided with an ICME; (2) Day 155, 2007, associated with a CIR; (3) day 201,

67 2007, which coincided with significant velocity gradient bisecting the $\sim 2°$ latitudinal

68 separation of the spacecraft [*Rouillard et al.*, 2009]; and (4) days 227 - 235, 2007. They

69 ascribed the poor correlation during the first portion of this last interval (days 227 - 231)

70 to temporal evolution of the solar wind source as it moved from under one spacecraft to

71 the other. Since the stream structure of the second half of this interval remained intact one

72 rotation later, they suggested that the poor correlation was due to spatial inhomogeneities.

2. The STEREO Orbits

73 The relative locations of the two STEREO spacecraft obviously play an important role

74 in understanding the large-scale correlation of solar wind parameters. Figure 1 summa-

75 rizes the heliocentric distance, latitude, and longitude of the spacecraft, together with the

76 differences between them. In the top panel, $R - 1$ is plotted, showing that the spacecraft

77 oscillate about values slightly less or more than 1 AU. These oscillations are synchronous

78 so that during mid/late 2007, 2008, and 2009 the spacecraft have a maximum radial sepa-

79 ration of ~ 0.13 AU. We can estimate the maximum temporal lag between the spacecraft

80 due to the radial separation using $\Delta t = \Delta r / v_{sw}$. Assuming $v_{sw} = 600$ km s^{-1}, we obtain

81 $\Delta t \sim 9$ hours. The temporal lag due to longitudinal effects obviously begins to dominate

82 once the spacecraft are separated by $\sim \frac{1 day}{27 days} \times 360° \sim 13°$. Following launch, the two

83 spacecraft maintained their position in the ecliptic plane, but as they moved farther apart,

84 their heliographic latitudinal separation began to oscillate, the amplitude of which became

progressively larger. The black curve in the middle panel summarizes this effect: Maximum latitudinal differences occurred at the shortly before the beginning of, and midway through each year. Finally, in the bottom panel, the inertial longitude of the spacecraft is shown, together with their monotonically-increasing azimuthal separation. Of particular note is that this separation is not strictly linear: Prior to, and during the early portion of each calendar year, the increase in separation is modest, whereas, for the remainder of the year, it is more pronounced.

In this study, we investigate the evolving cross correlation function (CCF) between solar wind velocity measurements at STEREO A and B. Unlike the previous study of *Opitz et al.* [2009], we do not assume and apply a phase lag between the measurements from which a correlation coefficient is computed, but rather compute the temporal phase lag between the two STEREO spacecraft that maximizes the CCF. To a first approximation, the results match our intuition and previous studies, that the phase lag increases linearly with the angular separation of the spacecraft; However, there are two interesting intervals where the phase lag "pauses." We use global MHD model solutions to show that these intervals are due to a combination of both temporal and spatial effects.

3. Analysis of STEREO in situ Bulk Solar Wind Speed Observations

In general, the CCF between two continuous functions is the integral of the complex conjugate of one variable and the time-shifted value of the other variable:

$$(f \star g)(\Delta t) = \int_{-\infty}^{\infty} f^*(\tau)g(\Delta t + \tau)d\tau \tag{1}$$

103 Extending this to real-valued discrete functions of finite length, which in this study

104 are the bulk solar wind velocities measured at the two spacecraft (v_A and v_B) over some

105 temporal lag, Δt, we can define the CCF to be:

$$
\begin{aligned}
(v_A \star v_B)(\Delta t) = = & \frac{\sum_{k=0}^{N-|\Delta t|-1}(v_{A,k+|\Delta t|} - \bar{v}_A)(V_{B,k} - \bar{v}_B)}{\sqrt{\left[\sum_{k=0}^{N-1}(v_{A,k} - \bar{v}_A)^2\right]\left[\sum_{k=0}^{N-1}(v_{B,k} - \bar{v}_B)^2\right]}} for L < 0 \\
= & \frac{\sum_{k=0}^{N-|\Delta t|-1}(v_{A,k} - \bar{v}_A)(v_{B,k+\Delta t} - \bar{v}_B)}{\sqrt{\left[\sum_{k=0}^{N-1}(v_{A,k} - \bar{v}_A)^2\right]\left[\sum_{k=0}^{N-1}(v_{B,k} - \bar{v}_B)^2\right]}} for L > 0 \quad (2)
\end{aligned}
$$

106 where $\bar{v}_A$ and $\bar{v}_B$ are the mean values of variables between 0 and $N-1$ [1].

107 Thus, for two real-valued functions (v_A and v_B), which differ only by a shift along the

108 time axis, we can compute the CCF for a range of time lags (Δt). Where the functions

109 match, the peaks and troughs become aligned, making a positive contribution to the sum-

110 mation, and the CCF is maximized. In the specific case of bulk solar wind velocities, which

111 are always positive, the CCF maximum is weighted more by the fast solar wind streams,

112 than the slow wind, since these contribute proportionately more to the summations.

113 Figure 2 illustrates graphically how the time shift that maximizes the CCF increases as

114 the angular separation of the spacecraft becomes larger. We can estimate how we would

115 expect the time lag (Δt) that maximizes the CCF to increase with angular separation

116 ($\Delta \lambda$). It is simply the fraction of a solar rotation by which the spacecraft are separated.

117 Thus, we anticipate that the phase lag should change by:

$$
\Delta t(hrs) = -\frac{27 \times 24}{360°}\Delta \lambda \quad (3)
$$

118 where we have chosen a negative decrease to reflect a convention that it is the amount

119 of time that measurements from spacecraft A must be shifted back in time to align with

spacecraft B. As a concrete example, at a separation of 55.5°, the predicted absolute phase

lag would be ~ 100 hrs, or a little over 4 days. It is worth noting that the synodic, rather

than the sidereal period is the appropriate interval to use, since the two spacecraft are

drifting apart from the Earth and not some fixed inertial point in space.

In Figure 3 (top), we have identified and plotted the phase lag of the peak of the

computed CCF as a function of spacecraft separation. A CCF was computed every 10^{-3}

years and each CCF was computed using a window of 0.1 years. The phase lag was

identified automatically by locating the peak in the CCF and all CCFs were visually

inspected to verify that the peak represented a pronounced maximum in the distribution.

The anticipated phase lag from equation (3) is shown by the dashed line. To a first

approximation, then the computed phase lag matches the simple formula. That is, the

phase lag increases linearly with time. However, two obvious deviations are apparent.

Since they represent intervals where the phase lag appears to "pause" from its trend

of increasing, we refer to them as "lulls." The first is centered on Carrington rotation

(CR) 2061, while the second is centered on CR 2069. Both span approximately the same

duration in longitude, $\sim 12.5°$, corresponding to ~ 3.5 months or 101 days. Whereas the

first has the appearance of a "pause," in the sense that the phase lag holds steady at

-45 hours before returning to its expected value, the second shows a significant reversal

in the trend of increasing lag: Where the predicted lag would have been -90 hours, the

computed lag was only -55 hours, a difference of 35 hours, or 19.4° in effective longitude.

In Figure 3 (bottom), we have plotted the value of the peak correlation coefficient at

that phase lag. Thus, until the spacecraft reached a separation of $\sim 75°$, the correlation

coefficient exceeded 0.6 and, for the majority of the time remained near 0.8. Beyond

~ 75°, as the peak correlation coefficient decreased, multiple peaks appeared, and, while it would have been possible to force a local phase lag that matched our expectations based on equation (3), the low value of the correlation coefficient would cast doubt on any inferences drawn.

4. Global MHD Model Solutions for the STEREO Mission

The first MHD models of the solar corona were developed almost 40 years ago [*Endler*, 1971; *Pneuman and Kopp*, 1971]. Over the years they have become progressively more sophisticated [*Steinolfson et al.*, 1982; *Linker et al.*, 1990; *Mikić and Linker*, 1994], culminating in models that include the photospheric field as a boundary condition [*Usmanov*, 1993; *Mikic et al.*, 1996; *Riley et al.*, 2001a; *Roussev et al.*, 2003]. Complementary efforts focusing on heliospheric models, where the inner boundary was placed beyond the outermost critical point, have also been pursued [*Dryer et al.*, 1978; *Pizzo*, 1978; *Smith and Dryer*, 1990; *Detman et al.*, 1991; *Odstrcil*, 1994]. Most recently, coronal and heliospheric models have been coupled [*Riley et al.*, 2001a, 2002; *Odstrcil et al.*, 2002; *Riley et al.*, 2003; *Odstrcil et al.*, 2004; *Manchester et al.*, 2006; *Riley et al.*, 2007] and more sophisticated descriptions of energy transport processes have been included [*Lionello et al.*, 2001; *Lionello et al.*, 2009].

We have computed global coronal and heliospheric polytropic MHD solutions spanning more than 35 years, and, in particular, for the entire STEREO mission to date (http://www.predsci.com/stereo). An important feature that makes our approach unique is the use of observed photospheric magnetograms to drive the solutions. Studies comparing model results with eclipses [*Mikic et al.*, 2002; *Mikić et al.*, 2007] as well as *in situ* observations at Ulysses and near Earth have shown that we can reproduce the basic

165   features of the solar corona and inner heliosphere [*Riley et al.*, 1996, 2001a, b, 2002, 2003;

166   *Riley*, 2007].

167   In general, our three-dimensional, time-dependent algorithm solves the following form

168   of the resistive MHD equations on a non-uniform grid in spherical coordinates:

$$\nabla \times \mathbf{B} = \frac{4\pi}{c}\mathbf{J}, \tag{4}$$

$$\nabla \times \mathbf{E} = -\frac{1}{c}\frac{\partial \mathbf{B}}{\partial t}, \tag{5}$$

$$\mathbf{E} + \frac{\mathbf{v} \times \mathbf{B}}{c} = \eta\mathbf{J}, \tag{6}$$

$$\frac{\partial \rho}{\partial t} + \nabla \cdot (\rho\mathbf{v}) = 0, \tag{7}$$

$$\frac{1}{\gamma - 1}\left(\frac{\partial T}{\partial t} + \mathbf{v} \cdot \nabla T\right) = -T\nabla \cdot \mathbf{v} + \frac{m_p}{2k\rho}S \tag{8}$$

$$\rho\left(\frac{\partial \mathbf{v}}{\partial t} + \mathbf{v} \cdot \nabla \mathbf{v}\right) = \frac{1}{c}\mathbf{J} \times \mathbf{B} - \nabla(p + p_w) + \rho\mathbf{g} + \nabla \cdot (\nu\rho\nabla\mathbf{v}), \tag{9}$$

$$S = (-\nabla \cdot \mathbf{q} - n_e n_p Q(T) + H_{\text{ch}}), \tag{10}$$

169   where $\mathbf{B}$ is the magnetic field, $\mathbf{J}$ is the electric current density, $\mathbf{E}$ is the electric field,

170   ρ, $\mathbf{v}$, p, and T are the plasma mass density, velocity, pressure, and temperature, $\mathbf{g} =$

171   $-g_0 R_S^2 \hat{\mathbf{r}}/r^2$ is the gravitational acceleration, η the resistivity, and ν is the kinematic

172   viscosity. Equation (10) contains the radiation loss function $Q(T)$, n_e and n_p are the

173   electron and proton number density (which are equal for a hydrogen plasma), m_p is the

174   proton mass, γ is the polytropic index, H_{ch} is the coronal heating term, and $\mathbf{q}$ is the heat

175   flux. The wave pressure term p_w in Eq. (9) represents the contribution due to Alfvén

176   waves and is evolved using the WKB approximation for time-space averaged Alfvén wave

177   energy density ϵ [*Mikić et al.*, 1999]. The method of solution of equation (6) through

178   (9), including the boundary conditions, has been described previously [*Mikić and Linker*,

179   1994; *Linker and Mikić*, 1997; *Lionello et al.*, 1999; *Mikić et al.*, 1999; *Linker et al.*, 2001;

180   *Lionello et al.*, 2009]. In the work presented here, however, we simplify these equations

181   by employing a "polytropic" energy equation, where $S = 0$ [*Usmanov*, 1993; *Mikic et al.*,

182   1996; *Usmanov*, 1996; *Linker et al.*, 1999; *Mikić et al.*, 1999; *Riley et al.*, 2001a, 2002, 2003;

183   *Roussev et al.*, 2003] and employ an empirical technique for deriving the speed profile for

184   the inner boundary of the heliospheric model. Although such an approximation is at odds

185   with observations (it requires that we set $\gamma = 1.05$ in the coronal model, for example), we

186   have found that that this approach for deriving solar wind speed is, at least currently, more

187   accurate than can be obtained from the more self-consistent thermodynamic approach.

188   Figure 4 compares model results with STEREO and ACE observations for CR 2060,

189   which occurred during one the intervals identified as "lulls." The solid lines show model

190   solutions, which were extracted by flying the spacecraft trajectories through the simulation

191   domain. We note that the relative phasing of the streams at the three locations is captured

192   in the model results. The fast stream centered on day 240, for example, is first seen

193   at STEREO A, then ACE (Earth), and finally at STEREO B. Moreover, the general

194   large-scale stream structure for this rotation is reproduced by the model: Generally slow

195   and variable wind during the first half, followed by a large stream at day 240, and two

196   smaller streams following it. The precise phasing of the modeled streams relative to the

197   observations does not match up well, however: The first stream is predicted to arrive

198   earlier than it actually does and the second stream is predicted to arrive later. Overall,

199   however, these relatively typical results match sufficiently well that the model can be used

200   to interpret the observations. The bottom panel summarizes the polarity of the radial

component of the magnetic field. Both model and observations suggest an essentially two-sector pattern for this rotation.

Figure 5 summarizes the computed coronal hole boundaries for CRs 2058 through 2063. These maps mark regions of open field lines (dark grey) and closed field lines (light grey) at the photosphere. We note that, during this time, there were well-defined polar coronal holes, together with equatorward extensions to these holes, as well as low and mid-latitude holes, not obviously connected to other open field regions. The quantitative steps taken to compute the speed profiles in the model are described by *Riley et al.* [2001a]. In brief, a velocity profile at the photosphere, consisting of fast wind everywhere with slow wind localized at the boundaries between the open and closed field lines, is mapped outward along the field lines to $30R_S$. Figure 6 shows the results of that mapping. Specifically, it shows the bulk radial solar wind velocity at $30R_S$ for each of these six rotations. The trajectories of Earth, STEREO A, and STEREO B are overlaid. Since Carrington longitude increases from left to right in each panel, time proceeds from right to left. Thus, with increasing time, the spacecraft sample progressively earlier Carrington longitudes.

The connection between the computed coronal holes in Figure 5 and the high-speed streams within Figure 6 can, at least qualitatively, be understood; however, it is clear that the topology of the field lines between $1R_S$ and $30R_S$ has added a great deal of complexity to the velocity map. From Figure 6, we note the following points. First, the spacecraft were essentially located at the same heliographic latitude during this interval. Certainly, based on the quality of the match shown in Figure 4, we could not reliably ascribe any spatial inhomogeneities to these modest separations. Second, the three high-

speed streams intercepted by all three spacecraft, initially at $\sim 120°$ in CR 2059 and $\sim 210°$ and $\sim 340°$ in CR 2060 drift westward in the ensuing rotations.

Figures 7 and 8 show coronal hole boundaries and speed profiles for CRs 2067 through 2072, which span the second "lull." For this interval, we note the following. First, the spacecraft were separated more substantially in heliographic latitude. Second, again, there was a westward progression of the high-speed streams that were intercepted by the spacecraft. Third, the stream boundaries tended to have a systematic tilt to them. This can be seen more clearly in the low-latitude coronal holes, which are orientated from SE to NW. The fast streams have a more complex profile, however, there is a tendency for STEREO A, which is at a higher heliographic latitude, to intercept the matching stream interface at a more westerly longitude.

5. Interpretation

There are two obvious ways that the linear relationship between time lag and the increasing longitude of the two STEREO spacecraft can be broken: temporal changes and/or spatial inhomogeneities. In the case of the latter, the pattern at the Sun does not change in time so that the structure of the solar wind in a frame rotating with the Sun is stationary; that is, it is strictly corotating. However, if the two spacecraft are not located at exactly the same heliographic latitude, they will intercept different plasma sources. Consider, for example, an idealized, elongated low-latitude coronal hole, oriented so that one end is in the SE and the other end lies in the NW. This is shown schematically in Figure 9. If STEREO A is located at a higher heliographic latitude than STEREO B, then the CH, and hence fast solar wind stream, will arrive slightly earlier than predicted since it is rooted in a more western source. Temporal effects can be understood in a similar way. If

a low-latitude CH evolves in time so that it shifts toward the west as the structure passes

from STEREO B to A, then the stream will arrive earlier than predicted by equation (3).

Both of these examples, thus, lead to the "lulls" we have identified in the data. Clearly,

in principle, it is possible for the opposite effects to take place: Structure that is oriented

from the NE to SW or temporal evolution of structure that tends to precess in the Car-

rington frame would drive larger time lags. Our model results, however, do not provide

any examples of this occurring during the STEREO timeframe. Instead, surrounding CR

2061, the general trend was for structures intercepted by the spacecraft to drift westward,

while surrounding CR 2070, both spatial and temporal effects likely contributed to the

"lulls." In particular, the stream interfaces were oriented from the SE to NW, so that

wind from the same coronal hole arrived earlier than would have been predicted, and the

coronal hole structure evolved such that the fast wind streams migrated westward.

As a final verification of this interpretation, we consider the first 6 Carrington rotations

of the STEREO mission. During this interval, the phase lag of the signals at the two

spacecraft matched the linear increase predicted by Equation (3). The computed solar

wind velocities at $30R_S$ for this interval are shown in Figure 10. During CR 2053 through

2055 the CCF was driven by a stable pattern involving two long-lived equatorial coronal

holes (at longitudes of $\sim 110°$ and $\sim 270°$). The spacecraft were not significantly separated

in latitude, and thus, we would not expect spatial inhomogeneities to drive a deviation in

the time lag. Moreover, there was no systematic evolution of the coronal holes during this

interval. Based on these results, then, we would not expect any deviations in the time lag

profile. During the second half of this interval, the wind sampled by the two spacecraft

was slow, variable, and unorganized. Again, there were no obvious systematic trends.

6. Summary

In this study, we have applied a cross-correlation analysis to STEREO A and B bulk solar wind velocity measurements for the period from launch through mid 2009. We found that, as with previous studies [*Podesta et al.*, 2008; *Opitz et al.*, 2009], there is a general trend for the phase lag between the streams to increase within increasing separation of the spacecraft. We also identified two intervals that deviated significantly from this trend. The first, centered around CR 2060, was previously identified by *Opitz et al.* [2009]. We used global MHD simulation results to understand these "lulls" in terms of both temporal evolution of the streams, as they swept first past B and then A, as well as spatial inhomogeneities, such that the two spacecraft, separated in latitude by up to $\sim 14°$ sampled different portions of the streams. Finally, beyond a separation of $\sim 80°$, the CCF peaked at values < 0.5, suggesting that from this point, correlation analysis must be applied and interpreted with considerably more caution.

Notes

1. The algorithm used to compute this function is available as part of the Interactive Data Language (IDL) numerical package (c_correlate.pro in the main library directory).

References

Detman, T. R., M. Dryer, T. Yeh, S. M. Han, and S. T. Wu, A time-dependent, three-dimensional MHD numerical study of interplanetary magnetic draping around plasmoids in the solar wind, *J. Geophys. Res.*, *96*, 9531–9540, doi:10.1029/91JA00443, 1991.

Dryer, M., Z. K. Smith, E. J. Smith, J. D. Mihalov, J. H. Wolfe, R. S. Steinolfson, and S. T. Wu, Dynamic MHD modeling of solar wind corotating stream interaction regions observed by Pioneer 10 and 11, *J. Geophys. Res.*, *83*, 4347–4352, doi: 10.1029/JA083iA09p04347, 1978.

Endler, F., Wechselwirkung zwischen Sonnenwind und koronalen Magnetfeldern, *Mitteilungen der Astronomischen Gesellschaft Hamburg*, *30*, 136–+, 1971.

Gosling, J. T., and S. J. Bame, Solar-wind speed variations 1964 - 1967: An autocorrelation analysis., *J. Geophys. Res.*, *77*, 12–26, doi:10.1029/JA077i001p00012, 1972.

Gosling, J. T., J. R. Asbridge, S. J. Bame, and W. C. Feldman, Solar wind speed variations - 1962-1974, *J. Geophys. Res.*, *81*, 5061–5070, doi:10.1029/JA081i028p05061, 1976.

Linker, J. A., and Z. Mikić, Extending coronal models to earth orbit, *Coronal Mass Ejections*, *99*, 269, edited by N. Crooker, J. Joselyn, and J. Feynmann, p. 269, AGU, Washington, D. C., 1997.

Linker, J. A., G. van Hoven, and D. D. Schnack, A three-dimensional simulation of a coronal streamer, *Geophys. Res. Lett.*, *17*, 2281–2284, doi:10.1029/GL017i013p02281, 1990.

Linker, J. A., R. Lionello, Z. Mikić, and T. Amari, Magnetohydrodynamic modeling of prominence formation within a helmet streamer, *J. Geophys. Res.*, *106*(A11), 25,165, 2001.

Linker, J. A., et al., Magnetohydrodynamic modeling of the solar corona during whole sun month, *J. Geophys. Res.*, *104*(A5), 9809, 1999.

Lionello, R., Z. Mikić, and J. A. Linker, Stability of algorithms for waves with large flows, *J. Comp. Phys.*, *152*(1), 346, 1999.

Lionello, R., J. A. Linker, and Z. Mikić, Including the transition region in models of the large-scale solar corona, *Ap. J.*, *546*(1), 542, 2001.

Lionello, R., J. A. Linker, and Z. Mikić, Multispectral Emission of the Sun During the First Whole Sun Month: Magnetohydrodynamic Simulations, *Ap. J.*, *690*, 902–912, doi:10.1088/0004-637X/690/1/902, 2009.

Manchester, W. B., A. J. Ridley, T. I. Gombosi, and D. L. Dezeeuw, Modeling the Sun-to-Earth propagation of a very fast CME, *Advances in Space Research*, *38*, 253–262, doi:10.1016/j.asr.2005.09.044, 2006.

Mikić, Z., and J. A. Linker, Disruption of coronal magnetic field arcades, *Ap. J.*, *430*, 898, 1994.

Mikic, Z., J. A. Linker, and J. A. Colborn, An MHD Model of the Solar Corona and Solar Wind, *BAAS*, *28*, 868–+, 1996.

Mikić, Z., J. A. Linker, D. D. Schnack, R. Lionello, and A. Tarditi, Magnetohydrodynamic modeling of the global solar corona, *Phys. Plasmas*, *6*(5), 2217, 1999.

Mikic, Z., J. A. Linker, R. Lionello, and P. Riley, Predicting the Structure of the Solar Corona During the December 4, 2002 Total Solar Eclipse, *AGU Fall Meeting Abstracts*, pp. A468+, 2002.

Mikić, Z., J. A. Linker, R. Lionello, P. Riley, and V. Titov, Predicting the Structure of the Solar Corona for the Total Solar Eclipse of March 29, 2006, in *Solar and Stellar Physics Through Eclipses*, *Astronomical Society of the Pacific Conference Series*, vol. 370, edited by O. Demircan, S. O. Selam, and B. Albayrak, pp. 299–+, 2007.

Odstrcil, D., Interactions of solar wind streams and related small structures, *J. Geophys. Res.*, *99*(A9), 17,653, 1994.

Odstrcil, D., J. A. Linker, R. Lionello, Z. Mikić, P. Riley, V. J. Pizzo, and J. G. Luh-
  mann, Merging of coronal and heliospheric numerical 2-d mhd models, *J. Geophys. Res.*,
  107(A12), DOI 10.1029/2002JA009,334, 2002.

Odstrcil, D., V. J. Pizzo, J. A. Linker, P. Riley, R. Lionello, and Z. Mikic, Initial coupling
  of coronal and heliospheric numerical magnetohydrodynamic codes, *JASTP*, *66*, 1311–
  1320, 2004.

Opitz, A., et al., Temporal Evolution of the Solar Wind Bulk Velocity at Solar Minimum
  by Correlating the STEREO A and B PLASTIC Measurements, *Sol. Phys.*, *256*, 365–
  377, doi:10.1007/s11207-008-9304-7, 2009.

Paularena, K. I., G. N. Zastenker, A. J. Lazarus, and P. A. Dalin, Solar wind plasma
  correlations between IMP 8, INTERBALL-1, and WIND, *J. Geophys. Res.*, *103*, 14,601–
  14,618, doi:10.1029/98JA00660, 1998.

Pizzo, V., A three-dimensional model of corotating streams in the solar wind. I - Theo-
  retical foundations, *J. Geophys. Res.*, *83*, 5563–5572, 1978.

Pneuman, G. W., and R. A. Kopp, Gas-Magnetic Field Interactions in the Solar Corona,
  Sol. Phys., *18*, 258–+, 1971.

Podesta, J. J., A. B. Galvin, and C. J. Farrugia, Correlation length of large-scale solar
  wind velocity fluctuations measured tangent to the Earth's orbit: First results from
  Stereo, *J. Geophys. Res.*, *113*, 9104–+, doi:10.1029/2007JA012865, 2008.

Richardson, J. D., F. Dashevskiy, and K. I. Paularena, Solar wind plasma correlations
  between L1 and Earth, *J. Geophys. Res.*, *103*, 14,619–14,630, doi:10.1029/98JA00675,
  1998.

Riley, P., Modeling corotating interaction regions: From the Sun to 1 AU, *JASTP*, *69*, 32–42, doi:10.1016/j.jastp.2006.06.008, 2007.

Riley, P., J. T. Gosling, L. A. Weiss, and V. J. Pizzo, The tilts of corotating interaction regions at midheliographic latitudes, *J. Geophys. Res.*, *101*(A11), 24,349, 1996.

Riley, P., J. A. Linker, and Z. Mikić, An empirically-driven global mhd model of the corona and inner heliosphere, *J. Geophys. Res.*, *106*(A8), 15,889, 2001a.

Riley, P., J. A. Linker, Z. Mikić, and R. Lionello, Mhd modeling of the solar corona and inner heliosphere: Comparison with observations, in *Space Weather, Geophysical Monograph Series*, vol. 125, edited by P. Song, H. J. Singer, and G. L. Siscoe, p. 159, AGU, Washington, DC, 2001b.

Riley, P., J. A. Linker, and Z. Mikić, Modeling the heliospheric current sheet: Solar cycle variations, *J. Geophys. Res.*, *107*(A7), DOI 10.1029/2001JA000,299, 2002.

Riley, P., Z. Mikić, and J. A. Linker, Dynamical evolution of the inner heliosphere approaching solar activity maximum: Interpreting ulysses observations using a global mhd model, *Ann. Geophys.*, *21*, 1347, 2003.

Riley, P., R. Lionello, Z. Mikić, J. Linker, E. Clark, J. Lin, and Y.-K. Ko, "Bursty" Reconnection Following Solar Eruptions: MHD Simulations and Comparison with Observations, *Ap. J.*, *655*, 591–597, doi:10.1086/509913, 2007.

Rouillard, A. P., et al., A Multispacecraft Analysis of a Small-Scale Transient Entrained by Solar Wind Streams, *Sol. Phys.*, *256*, 307–326, doi:10.1007/s11207-009-9329-6, 2009.

Roussev, I. I., T. I. Gombosi, I. V. Sokolov, M. Velli, W. Manchester, D. L. DeZeeuw, P. Liewer, G. Tóth, and J. Luhmann, A Three-dimensional Model of the Solar Wind Incorporating Solar Magnetogram Observations, *Ap. J. Lett.*, *595*, L57–L61, 2003.

Smith, Z., and M. Dryer, Mhd study of temporal and spatial evolution of simulated interplanetary shocks in the ecliptic-plane within 1 au, *Sol. Phys.*, *129*, 387, 1990.

Steinolfson, R. S., S. T. Suess, and S. T. Wu, The steady global corona, *Ap. J.*, *255*, 730–742, doi:10.1086/159872, 1982.

Usmanov, A. V., A global numerical 3-D MHD model of the solar wind, *Sol. Phys.*, *146*, 377–396, doi:10.1007/BF00662021, 1993.

Usmanov, A. V., A global 3-d mhd solar wind model with alfven waves, *International Solar Wind 8 Conference*, *382*, 141, 1996.
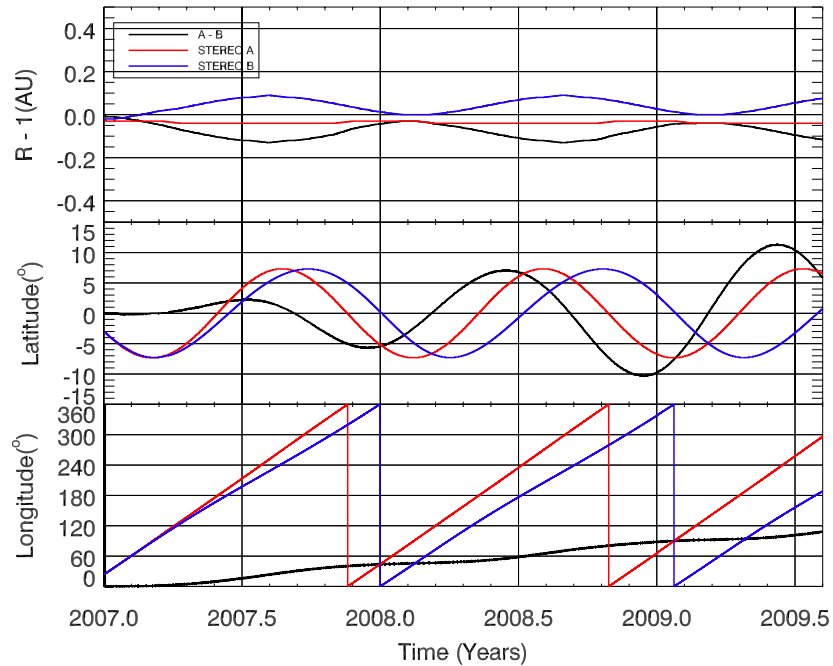
Figure 1. Ephemeris data for STEREO mission. In each panel, the red curve corresponds to the location of STEREO A, the blue curve to the location of STEREO B, and the black curve to the difference between them. (Top) The heliocentric location of the spacecraft, plotted relative to 1 AU; (Middle) The heliographic latitude of the spacecraft; and (Bottom) the heliographic, inertial longitude of the spacecraft.
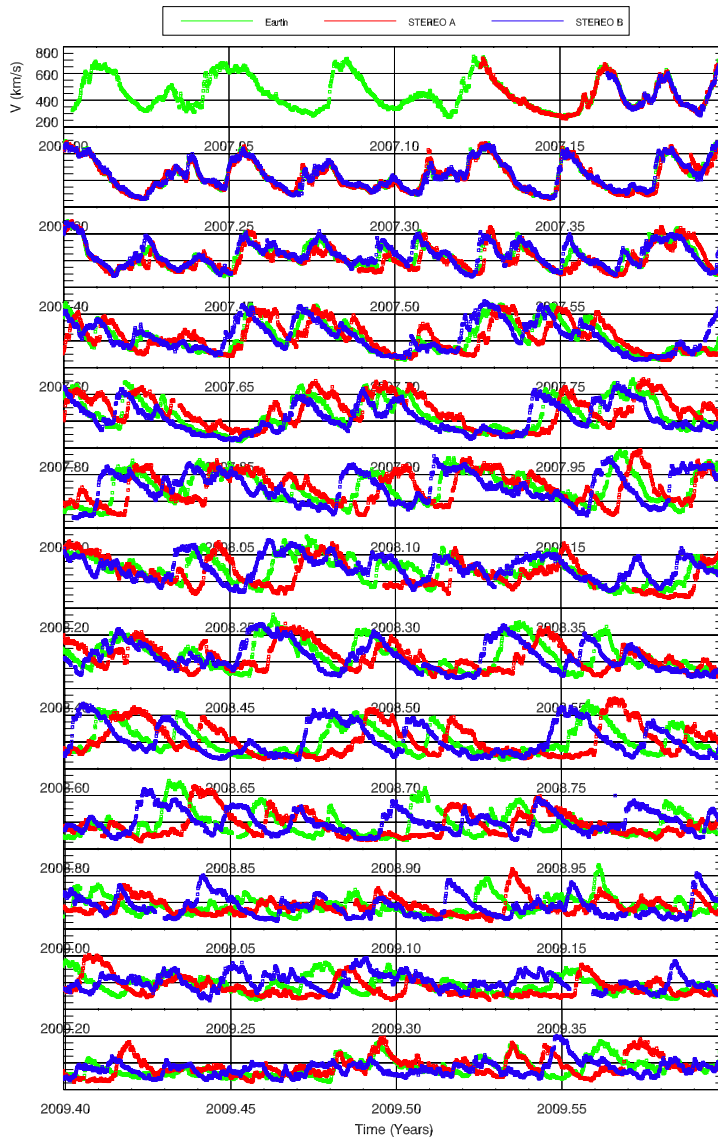
Figure 2.   Bulk solar wind speed from 2007.0 (top) through 2009.5 (bottom). Green, red, and blue correspond to Earth, STEREO A, and STEREO B, respectively. A movie illustrating the evolution of these streams can be viewed/downloaded at http://www.predsci.com/stereo/movies/.
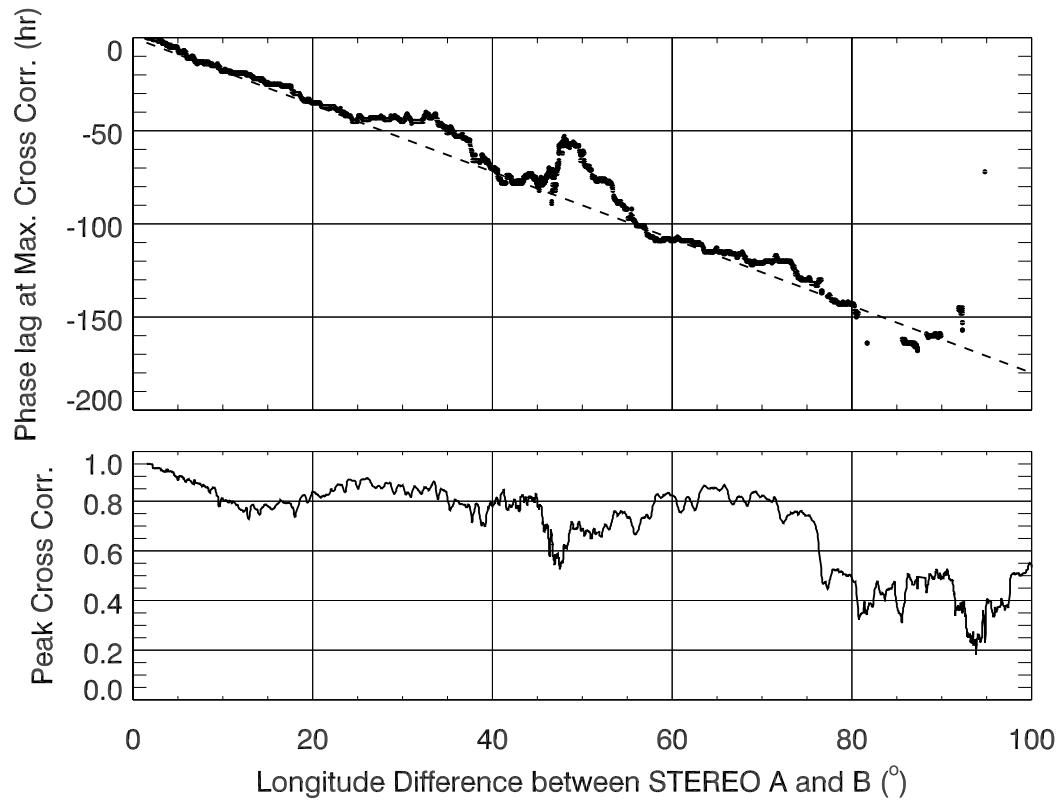
Figure 3. (Top) The temporal phase lag that maximizes the cross correlation function (CCF) between the solar wind velocities measured at STEREO A and B, plotted as a function of longitudinal separation of the spacecraft. (Bottom) The correlation coefficient corresponding to the phase lag in the plot above.
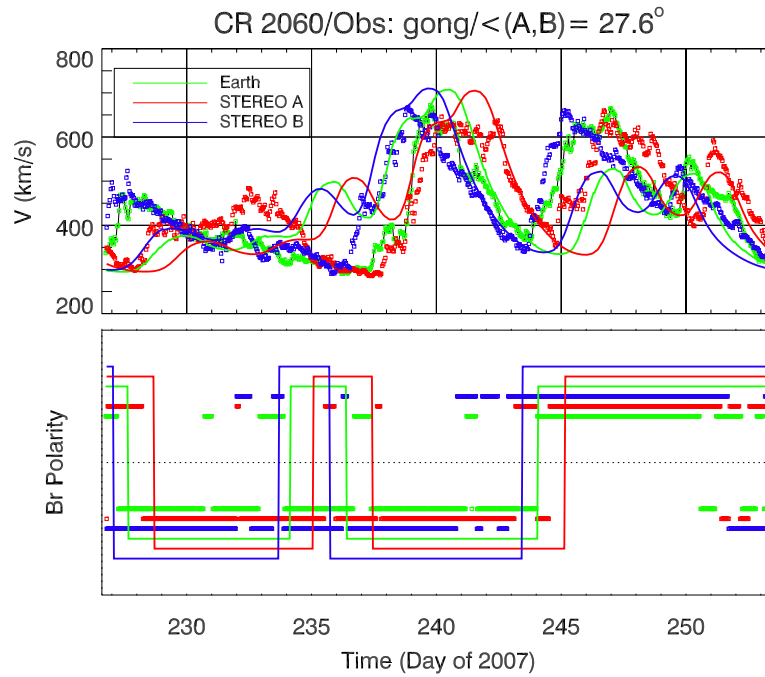
Figure 4.   Comparison of model results with (Top) *in situ* speed and (Bottom) radial IMF polarity for Carrington rotation (CR) 2060. The solid lines are model results and the symbols are *in situ* measurements from ACE (green), STEREO A (red), and STEREO B (blue). The amplitude of polarities have been adjusted to more easily show the variations at each spacecraft; there is no physical significance, however, to them.
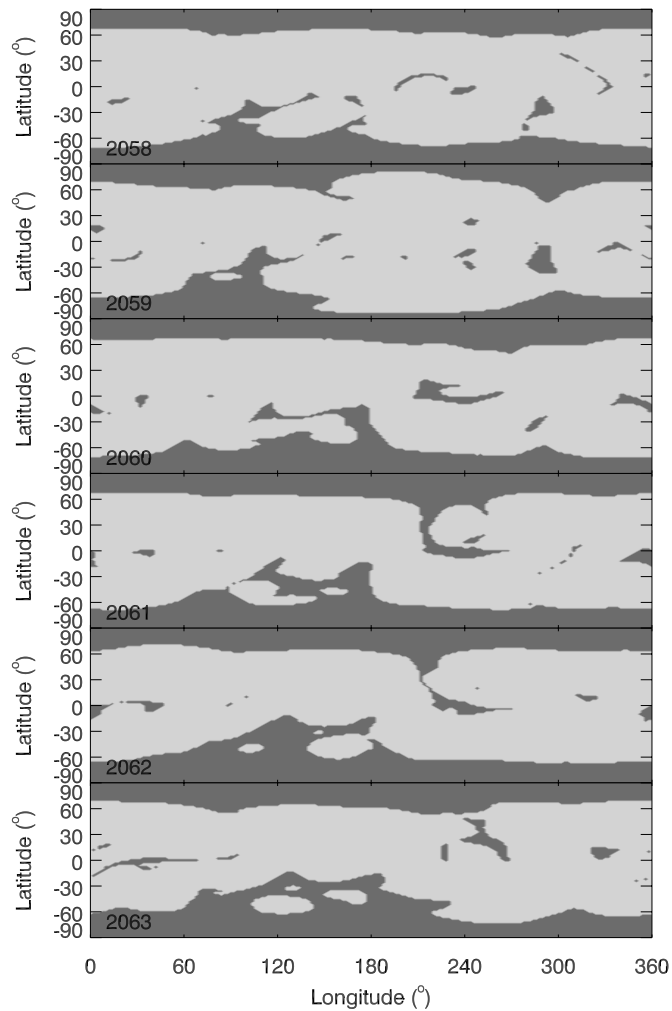
Figure 5. The computed coronal holes for CRs 2058 through 2063. These were obtained by tracing magnetic field lines outward from the photosphere and into the heliosphere. If the field line returned to the photosphere, it was labeled "closed" and shaded light grey, whereas if it reached the outer radial boundary of the simulation domain, it was labeled "open" and shaded dark grey.
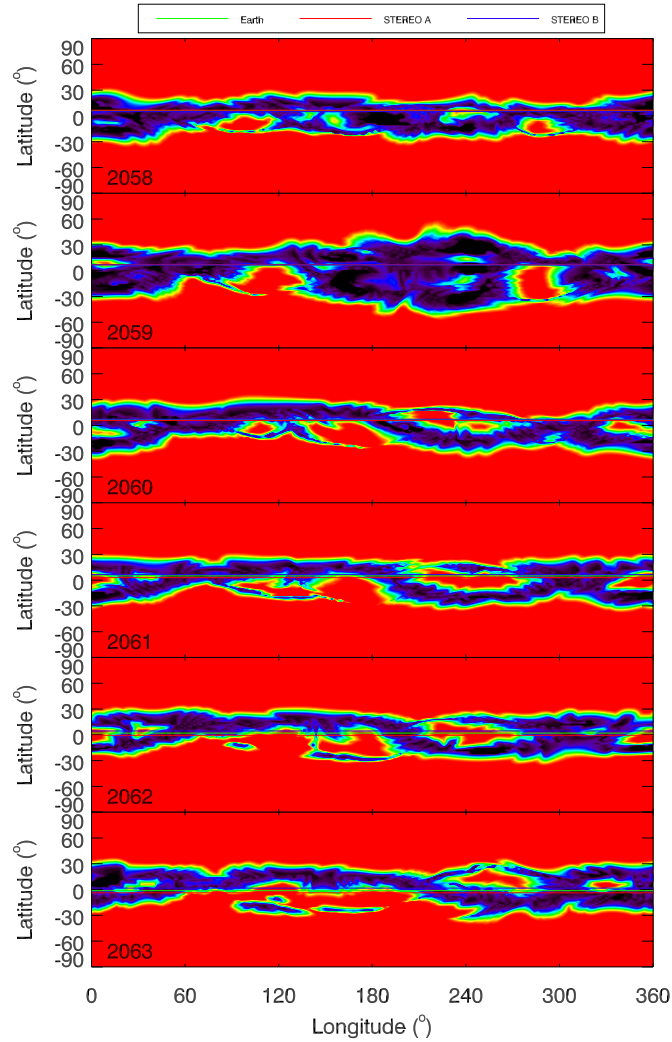
Figure 6.   The computed radial solar wind velocities for CRs 2058 through 2063. These were obtained by mapping a photospheric velocity profile (see *Riley et al.* [2001a] for details) outward along open field lines to $30R_S$. Red corresponds to ~ 750 km s^{-1}, while black corresponds to ~ 350 km s^{-1}.
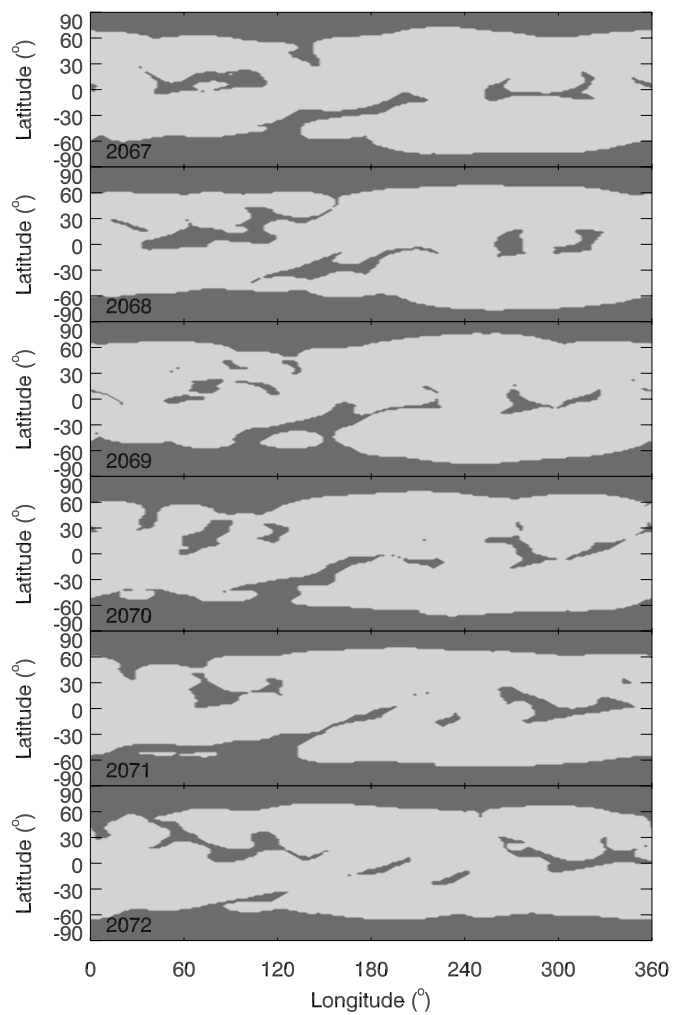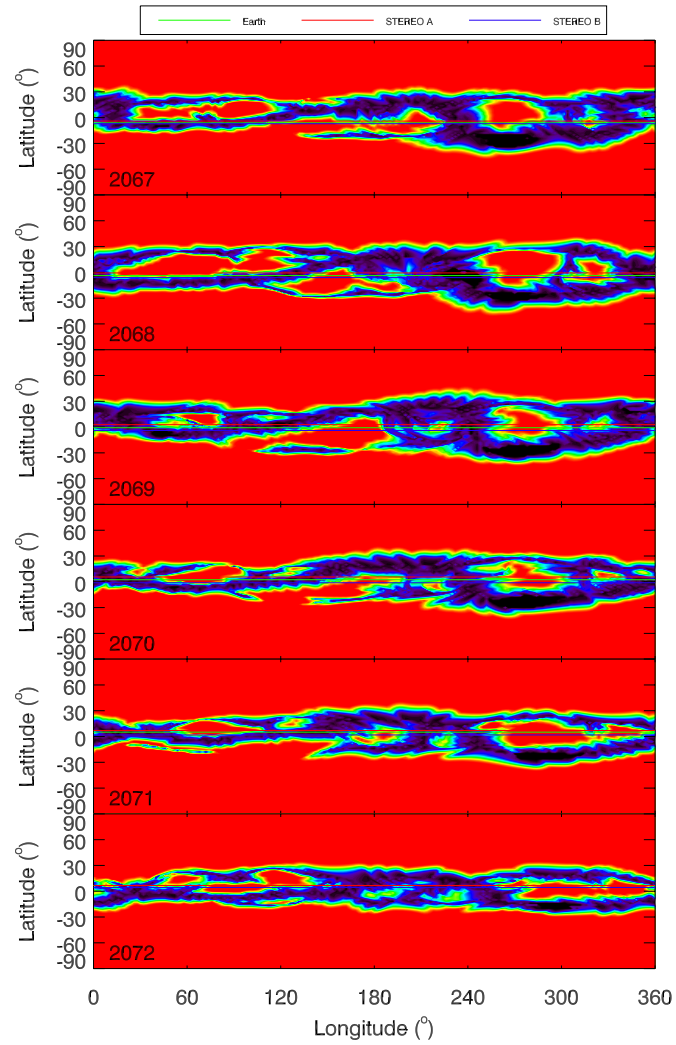
Figure 7.   As Figure 5 for CRs 2067 through 2072.
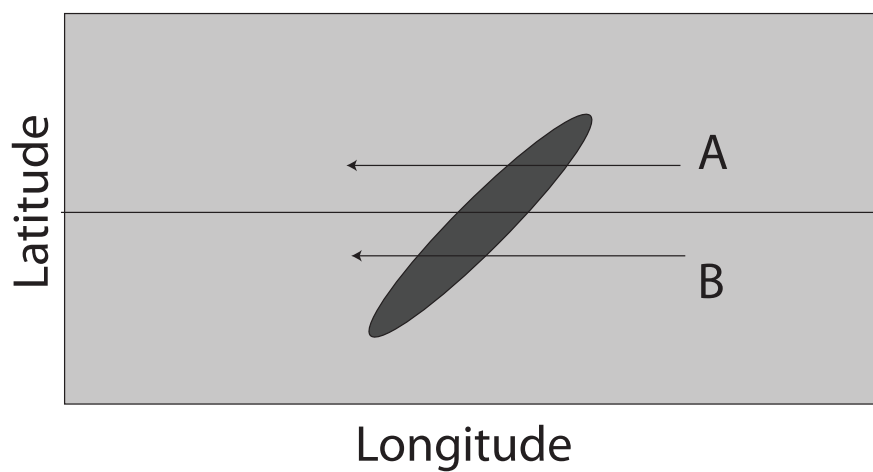
Figure 8. As Figure 6 for CRs 2067 through 2072.

Figure 9. Schematic illustration of how the orientation of a coronal hole can affect the phase lag between STEREO A and B. The trajectory of the two spacecraft through the coronal hole are marked by horizontal arrows.
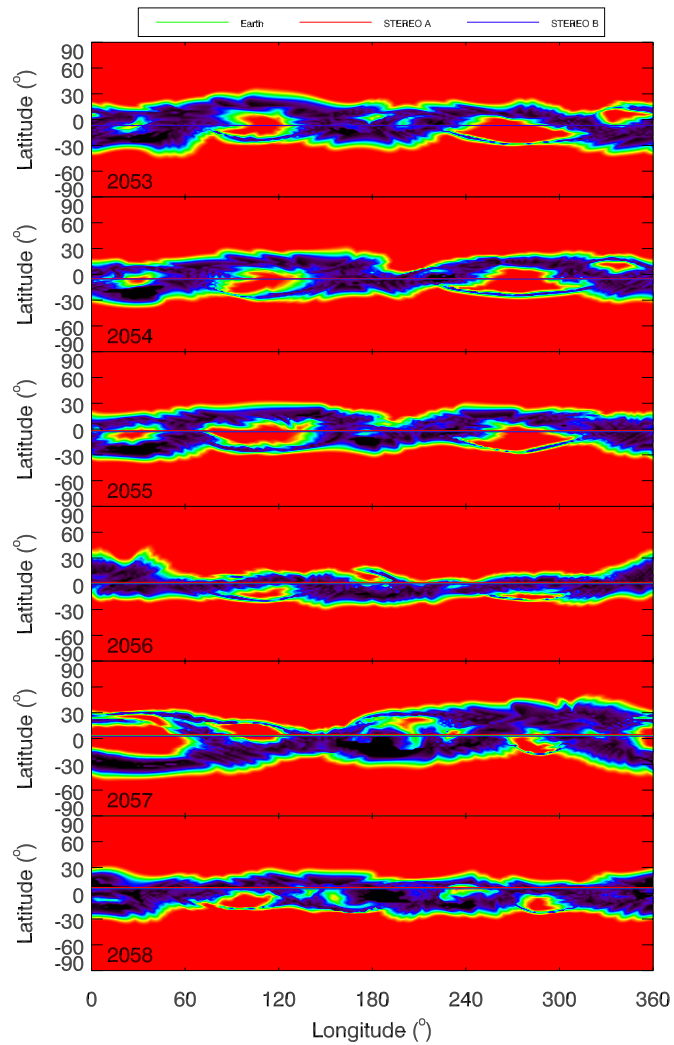
Figure 10.   As Figure 6 for CRs 2053 through 2058.